Acta Mechanica Solida Sinica (2024) 37:271–284
https://doi.org/10.1007/s10338-023-00454-4

Theoretical Analysis of the Buckling Behaviors of Inhomogeneous Shape Memory Polymer Composite Laminates Considering Prestrains

Hanxing Zhao[1] · Pengyu Cao[1] · Fengfeng Li[2] · Xin Lan[1] · Liwu Liu[2] · Yanju Liu[2] · Jinsong Leng[1]

Received: 11 July 2023 / Revised: 28 November 2023 / Accepted: 29 November 2023 / Published online: 12 February 2024

Abstract
The mismatch in thermal expansion coefficients between the fiber-rich and resin-rich regions of a shape memory polymer composite (SMPC) laminate, along with the residual strain during SMPC fabrication, results in buckling deformation of the inhomogeneous laminate. This paper presents a macroscopic model for buckling of an inhomogeneous SMPC laminate under initial biaxial prestrains. Both linear and nonlinear buckling analyses are carried out using the energy method. The influences of prestrain biaxiality, temperature, and ply angle on the buckling wavelength, critical buckling prestrain, and buckling amplitude are calculated. The results demonstrate that the critical buckling wavelength of the SMPC laminate is independent of the prestrain, while the amplitude is almost independent of temperature. In addition, the optimal fiber stacking configuration with the maximum critical buckling prestrains of inhomogeneous SMPC laminates is determined by a genetic algorithm.

Keywords Shape memory polymer composite · Buckling behavior · Inhomogeneous laminate · Biaxial prestrains

1 Introduction

Shape memory polymer (SMP) is a kind of material that can undergo large macroscopic deformation in response to external stimuli, such as changes in temperature, electric field, light, magnetic field, moisture, or even pH [1–5]. SMP has advantages of large deformation capacity, low cost and density, good processability, and adjustable glass transition temperature (T_g). However, the mechanical properties of SMP limit its applications to some extent [6–9]. Therefore, reinforcements, which can be particles or fibers, are embedded in the SMP matrix to fabricate shape memory polymer composites (SMPCs). SMPCs have good shape memory properties, additional functionality due to the type of reinforcements, and improved modulus and strength compared to SMPs [10–12].

✉ Yanju Liu
yj_liu@hit.edu.cn

✉ Jinsong Leng
lengjs@hit.edu.cn

[1] Centre of Composite Materials and Structures, Harbin Institute of Technology (HIT), Harbin 150080, China

[2] Department of Astronautical Science and Mechanics, Harbin Institute of Technology (HIT), Harbin 150001, China

At present, continuous fiber-reinforced SMPC has been widely used in aerospace fields [13–18], and the related applications have gradually changed from functional components to structural–functional integrative components, which requires SMPCs with excellent mechanical properties. With the development of composite manufacturing technologies, dozens of technical processes have been developed, among which the manufacturing technology based on continuous fiber-reinforced prepreg has become the preferred method for the preparation of high-performance composites. Unlike general composites, the fiber volume fraction of SMPC should be relatively low ($< 30\%$) to maintain its shape memory property [8]. Therefore, it is necessary to lay SMP films between the prepreg layers to adjust the fiber volume fraction. As a result, fibers will not be evenly distributed in the resin matrix, and the existing fiber-rich region and resin-rich region contribute to the inhomogeneity of the SMPC laminate. Due to the mismatch in coefficients of thermal expansion (CTE) between the fiber-rich region and resin-rich region and the residual strain during the curing process [19, 20], the initial prestrain will exist in the inhomogeneous SMPC laminate, resulting in buckling deformation of the composite [21]. However, few studies have been conducted on this phenomenon.

There have been many studies on the buckling behavior of inhomogeneous laminates, which are simplified into laminate layers bonded with resin layers. Sironic and Briscoe et al. [22, 23] studied the buckling behaviors of isotropic rectangular plates on elastic foundations under in-plane compressive loads using a two-parameter foundation model. Behzad et al. [24] studied the buckling behaviors of orthotropic laminated plates on elastic foundations under in-plane bending loads. Yang, Cao, and Topal et al. [25–27] investigated the buckling behaviors of elastic foundation-supported laminated plates with specific fiber plying angles based on classical lamination theory (CLT) and obtained the relationships between buckling loads and elastic foundation constants. The results showed that the critical buckling load increased with increasing elastic modulus of the foundation.

In the above-mentioned studies, the laminated plates are simplified into isotropic or orthotropic layers, where the effect of fiber plying angles on critical buckling loads could not be considered. Moreover, the effect of initial prestrain was not considered, which, however, cannot be ignored during the curing process. In addition, as typical temperature-sensitive materials, the mechanical properties of SMP and SMPC are closely related to temperature, so temperature has a great influence on the buckling behaviors of inhomogeneous SMPC laminates. Therefore, relevant fundamental theoretical research on the buckling behaviors of inhomogeneous SMPC laminates considering prestrains is urgently needed.

In this paper, a macroscopic buckling model of inhomogeneous SMPC laminates under initial biaxial prestrains is established. The linear and nonlinear buckling analyses are carried out using the energy method. The influences of prestrain biaxiality, temperature, and fiber ply angle on the buckling wavelength, critical buckling prestrain, and buckling amplitude are then calculated. Finally, the fiber stacking configurations of the inhomogeneous SMPC laminates are optimized using a genetic algorithm.

2 Theoretical Model of the Inhomogeneous SMPC

2.1 Description of the Model

To study the macroscopic nonlinear buckling behaviors of the aforementioned inhomogeneous SMPC laminate under initial uniform in-plane prestrains, a simplified model is utilized. This model consists of an upper part, which represents the SMPC laminated plate, and a bottom part, which represents the SMP matrix with a finite thickness, as shown in Fig. 1. The resin matrix is assumed to be isotropic and perfectly bonded to the SMPC laminate, and the laminated plate is subjected to uniform in-plane biaxial prestrains. The thicknesses of the laminate and resin are h and H, respectively.

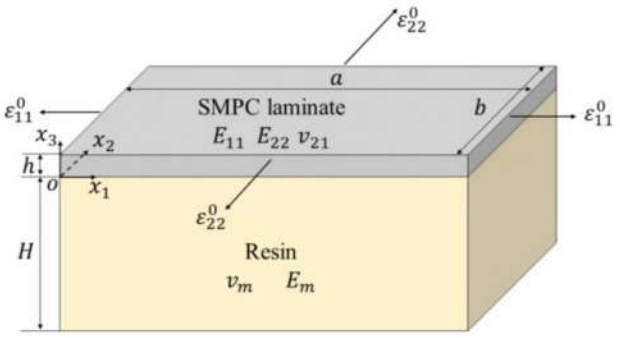

Fig. 1 Schematic of the inhomogeneous SMPC laminate with prestrains

Only the $o - x_1x_2$ plane of the laminated plate is subjected to uniform in-plane biaxial prestrains ε_{11}^0 and ε_{22}^0, which are probably caused by the residual stresses or a mismatch in thermal expansion coefficients between the laminate and resin matrix during curing. The SMPC laminate is assumed to be in the plane stress state.

A Cartesian coordinate system ($o-x_1x_2x_3$) is established, where the $o - x_1x_2$ plane lies at the interface of the SMPC laminate and resin matrix, and the x_3-axis is oriented perpendicular to the surface of the laminate, pointing upwards. It is worth noting that prestrain control, rather than prestress control, is selected as the loading mode in this study because the prestress and prestrain can be easily converted between each other using the stiffness of the material. The strain energies of the SMPC laminate and resin matrix during buckling are then calculated by the energy method, and the key parameters can be obtained by the variational method.

2.2 The Strain Energy of the Laminate

The von Karman nonlinear elastic plate theory is used to model the laminate. The expressions between the membrane strains and displacements are [28]:

$$\begin{cases} \varepsilon_{11} = \varepsilon_{11}^0 + \frac{\partial u}{\partial x_1} + \frac{1}{2}\left(\frac{\partial w}{\partial x_1}\right)^2 \\ \varepsilon_{22} = \varepsilon_{22}^0 + \frac{\partial v}{\partial x_2} + \frac{1}{2}\left(\frac{\partial w}{\partial x_2}\right)^2 \\ \varepsilon_{12} = \frac{\partial u}{\partial x_2} + \frac{\partial v}{\partial x_1} + \frac{\partial w}{\partial x_1}\frac{\partial w}{\partial x_2} \end{cases} \tag{1}$$

$$\begin{cases} \kappa_{11} = -\frac{\partial^2 w}{\partial x_1^2} \\ \kappa_{22} = -\frac{\partial^2 w}{\partial x_2^2} \\ \kappa_{12} = -2\frac{\partial^2 w}{\partial x_1 \partial x_2} \end{cases} \tag{2}$$

where ε_{11}^0 and ε_{22}^0 are the in-plane prestrains caused by residual stresses or a mismatch in thermal expansion coefficients between the SMPC laminate and resin matrix, which can be simplified as homogeneous in-plane strains. $\{u\ v\ w\}$ is the displacement vector of the SMPC laminate. It should be noted

that the strains in the above equations contain the nonlinear term of w because a moderately large deflection will lead to a change in the membrane length of the laminate.

According to CLT, the internal forces and moments of composite laminated plates can be expressed as

$$\begin{Bmatrix} N \\ M \end{Bmatrix} = \begin{bmatrix} A & B \\ B & D \end{bmatrix} \begin{Bmatrix} \varepsilon \\ \kappa \end{Bmatrix} \tag{3}$$

where the expressions for these stiffness matrices of laminates ($\boldsymbol{A}$, $\boldsymbol{B}$, and $\boldsymbol{D}$) with different ply stacking configurations are shown in Section S1 (Supplementary Information). $\boldsymbol{N}$ and $\boldsymbol{M}$ are the internal force matrix and internal moment matrix of a unit length on the cross section of the laminate.

Assuming that the shear stresses at the laminate/resin interface are P_1 and P_2 (in the x_1- and x_2-directions), and the normal stress is P_3. Omitting the body forces, the equilibrium equations expressed in terms of resultant force and moment are as follows:

$$N_{\alpha\beta,\beta} + P_\alpha = 0 \tag{4}$$

$$M_{\alpha\beta,\alpha\beta} + P_3 = 0 \tag{5}$$

where the Greek indices α and β take the values 1 and 2. Substituting Eq. (3) into Eqs. (4) and (5) yields the following equilibrium equations between the interfacial stress and the displacement of the SMPC laminate:

$$\begin{bmatrix} L_{11} & L_{12} & L_{13} \\ L_{12} & L_{22} & L_{23} \\ L_{13} & L_{23} & L_{33} \end{bmatrix} \begin{Bmatrix} u \\ v \\ w \end{Bmatrix} = \begin{Bmatrix} P_1 \\ P_2 \\ P_3 \end{Bmatrix} \tag{6}$$

The operator can be expressed as follows:

$$\begin{cases} L_{11} = A_{11}\frac{\partial^2}{\partial x_1^2} + 2A_{16}\frac{\partial^2}{\partial x_1 \partial x_2} + A_{66}\frac{\partial^2}{\partial x_2^2} \\ L_{12} = A_{16}\frac{\partial^2}{\partial x_1^2} + (A_{12} + A_{66})\frac{\partial^2}{\partial x_1 \partial x_2} + A_{26}\frac{\partial^2}{\partial x_2^2} \\ L_{22} = A_{66}\frac{\partial^2}{\partial x_1^2} + 2A_{26}\frac{\partial^2}{\partial x_1 \partial x_2} + A_{22}\frac{\partial^2}{\partial x_2^2} \\ L_{33} = D_{11}\frac{\partial^4}{\partial x_1^4} + 4D_{16}\frac{\partial^4}{\partial x_1^3 \partial x_2} + 2(D_{12} + 2D_{66})\frac{\partial^4}{\partial x_1^2 \partial x_2^2} \\ \qquad +4D_{26}\frac{\partial^4}{\partial x_1 \partial x_2^3} + D_{22}\frac{\partial^4}{\partial x_2^4} \\ L_{13} = -B_{11}\frac{\partial^3}{\partial x_1^3} - 3B_{16}\frac{\partial^3}{\partial x_1^2 \partial x_2} - (B_{12} + 2B_{66})\frac{\partial^3}{\partial x_1 \partial x_2^2} \\ \qquad -B_{26}\frac{\partial^3}{\partial x_2^3} \\ L_{23} = -B_{16}\frac{\partial^3}{\partial x_1^3} - (B_{12} + 2B_{66})\frac{\partial^3}{\partial x_1^2 \partial x_2} - 3B_{26}\frac{\partial^3}{\partial x_1 \partial x_2^2} \\ \qquad -B_{22}\frac{\partial^3}{\partial x_2^3} \end{cases} \tag{7}$$

The laminated plate will begin to buckle when the pre-strain ε^0 reaches a critical value, resulting in a specific buckling mode shape. Both the static method and the energy method can be used to derive the same equilibrium differential equations and solve this problem. However, for practical problems, especially post-buckling problems, solving the equilibrium differential equations is always challenging. Nevertheless, the problem can be greatly simplified when using the energy method to approximate the solution. Therefore, the nonlinear post-buckling behaviors of the inhomogeneous SMPC are determined by the energy method in this study.

During the pre-buckling state, the laminated plate undergoes linear deformation and remains flat. It is assumed that the post-buckling morphology of the laminated plate is a strip mode, and the deflection $w(x_1, x_2)$ can be expressed as

$$w(x_1, x_2) = A\cos(kx_1) \tag{8}$$

where A is the amplitude, and the buckling wavelength can be expressed as $\lambda = 2\pi/k$. Because the modulus of the laminate is much larger than that of the resin matrix, Huang et al. showed that the shear stress at the laminate/resin interface can be ignored [29], that is, $P_1 = P_2 = 0$. Substituting Eq. (8) into Eq. (6), the in-plane displacements u and v of the laminated plate can be solved as

$$u = \frac{A^2 k}{8}\sin(2kx_1),\ v = 0 \tag{9}$$

The components of strain $\varepsilon_{\alpha\beta}$ and $\kappa_{\alpha\beta}$ can be obtained by substituting Eqs. (8) and (9) into Eqs. (1) and (2). When buckling occurs, the surface strain energy per unit area of the laminated plate caused by in-plane deformation is

$$U_s = \frac{k}{4\pi b}\int_{x_1=0}^{2\pi/k}\int_{x_2=0}^{b}(N_1\varepsilon_1 + N_2\varepsilon_2 + N_{12}\varepsilon_{12})\mathrm{d}x_1\mathrm{d}x_2 \tag{10}$$

where $N_1\varepsilon_1 + N_2\varepsilon_2 + 2N_{12}\varepsilon_{12}$ can be expressed in terms of the stiffness coefficients and strains of the laminate as

$$\begin{aligned} &N_1\varepsilon_1 + N_2\varepsilon_2 + N_{12}\varepsilon_{12} \\ &= A_{11}{\varepsilon_{11}}^2 + 2A_{12}\varepsilon_{11}\varepsilon_{22} \\ &\quad + A_{22}{\varepsilon_{22}}^2 + 2A_{16}\varepsilon_{12}\varepsilon_{11} + 2A_{26}\varepsilon_{12}\varepsilon_{22} \\ &\quad + 2A_{66}{\varepsilon_{12}}^2 + B_{11}\kappa_{11}\varepsilon_{11} + B_{12}(\kappa_{22}\varepsilon_{11} \\ &\quad + \kappa_{11}\varepsilon_{22}) + B_{22}\kappa_{22}\varepsilon_{22} \\ &\quad + B_{16}(\kappa_{12}\varepsilon_{11} + \kappa_{11}\varepsilon_{12}) + B_{26}(\kappa_{12}\varepsilon_{22} \\ &\quad + \kappa_{22}\varepsilon_{12}) + B_{66}\varepsilon_{12}\kappa_{12} \end{aligned} \tag{11}$$

The bending strain energy U_b per unit area of the laminate caused by flexural deformation can be calculated as

$$U_b = \frac{k}{4\pi b}\int_{x_1=0}^{2\pi/k}\int_{x_2=0}^{b}(M_1\kappa_1 + M_2\kappa_2 + M_{12}\kappa_{12})\mathrm{d}x_1\mathrm{d}x_2 \tag{12}$$

where $M_1\kappa_1 + M_2\kappa_2 + 2M_{12}\kappa_{12}$ can also be expressed in terms of the stiffness coefficients and strains of the laminate as

$$\begin{aligned} &M_1\kappa_1 + M_2\kappa_2 + M_{12}\kappa_{12} \\ &= D_{11}{\kappa_{11}}^2 + 2D_{12}\kappa_{22}\kappa_{11} \\ &\quad + D_{22}{\kappa_{22}}^2 + 2D_{16}\kappa_{11}\kappa_{12} + 2D_{26}\kappa_{12}\kappa_{22} \\ &\quad + 2D_{66}{\kappa_{12}}^2 + B_{11}\varepsilon_{11}\kappa_{11} + B_{12}(\varepsilon_{11}\kappa_{22} + \varepsilon_{22}\kappa_{11}) \\ &\quad + B_{22}\varepsilon_{22}\kappa_{22} + B_{16}(\kappa_{11}\varepsilon_{12} + \kappa_{12}\varepsilon_{11}) \\ &\quad + B_{26}(\kappa_{22}\varepsilon_{12} + \kappa_{12}\varepsilon_{22}) + B_{66}\varepsilon_{12}\kappa_{12} \end{aligned} \tag{13}$$

Therefore, the expression of $U_l = U_s + U_b$ can be obtained by substituting the expressions of $\varepsilon_{\alpha\beta}$ and $\kappa_{\alpha\beta}$ into Eqs. (10) and (12), so we can calculate that

$$\begin{aligned} U_l = \frac{1}{2}\Bigg[&\frac{A_{11}}{16}k^4A^4 + \frac{A_{11}\varepsilon_{11}^0 + A_{12}\varepsilon_{22}^0}{2}k^2A^2 + A_{11}{\varepsilon_{11}^0}^2 \\ &+ 2A_{12}\varepsilon_{11}^0\varepsilon_{22}^0 + A_{22}{\varepsilon_{22}^0}^2\Bigg] + \frac{1}{4}A^2k^4D_{11} \end{aligned} \tag{14}$$

2.3 The Strain Energy of the Resin Matrix

Since the resin matrix is too thick to be considered a plane stress problem, the strain energy per unit area of the matrix can be expressed as

$$U_r = \frac{k}{4\pi b}\int_{x_1=0}^{2\pi/k}\int_{x_2=0}^{b}\int_{x_3=0}^{-H}\sigma_{ij}^r\varepsilon_{ij}^r\mathrm{d}x_1\mathrm{d}x_2\mathrm{d}x_3 \tag{15}$$

where i and j take the values 1, 2, and 3, and follow the Einstein summation convention (similarly hereinafter). σ_{ij}^r and ε_{ij}^r are the stress and strain components of the resin matrix, which are functions of the (x_1, x_2, x_3) coordinates.

Omitting the body force of the resin matrix, the displacement equilibrium equation can be expressed as the Lamé–Navier form [28]

$$(1-2\nu_r)\nabla^2u_i^r + u_{j,ji}^r = 0 \tag{16}$$

where ν_r is Poisson's ratio of the resin matrix. Because the shear stress at the laminate/resin interface can be ignored and the normal displacements of the upper surface of the matrix resin and the bottom surface of the laminate are continuous, the following boundary conditions can be obtained:

$$\begin{aligned} &P_1 = P_2 = 0,\ u_3^r = w(x_1, x_2),\ \text{at } x_3 = 0 \\ &\sigma_{ij}^r = 0,\ \text{at } x_3 = -H \end{aligned} \tag{17}$$

The displacement components u_i^r are assumed to be [30]

$$\begin{cases} u_1^r = B(x_3)\sin(kx_1) \\ u_2^r = 0 \\ u_3^r = C(x_3)\cos(kx_1) \end{cases} \tag{18}$$

Substituting Eq. (18) into the displacement equilibrium equation of the resin matrix Eq. (16), together with the boundary conditions of Eq. (17), the expressions for $B(x_3)$ and $C(x_3)$ can thus be calculated as

$$\begin{aligned} B(x_3) &= \frac{(2\nu_r - 1 + kx_3)Ae^{\frac{x_3}{x_3+H}}}{2(1-\nu_r)} \\ C(x_3) &= \frac{(2-2\nu_r + kx_3)Ae^{\frac{x_3}{x_3+H}}}{2(1-\nu_r)} \end{aligned} \tag{19}$$

For an isotropic resin matrix, the strain–displacement relationship and stress–strain relationship are

$$\varepsilon_{ij} = \frac{1}{2}\left(\frac{\partial u_i}{\partial x_j} + \frac{\partial u_j}{\partial x_i}\right) \tag{20}$$

$$\sigma_{ij} = \frac{E_r}{1+\nu_r}\varepsilon_{ij} + \frac{\nu_r E_r}{(1+\nu_r)(1-2\nu_r)}(\varepsilon_{11} + \varepsilon_{22} + \varepsilon_{33})\delta_{ij} \tag{21}$$

where δ_{ij} is the Kronecker symbol. Substituting Eqs. (18)–(21) into Eq. (15) yields the expression for U_r

$$U_r = \frac{A^2kE_r}{16(1-\nu_r^2)}\left[\frac{(3-4\nu_r)[-4Hk + 2\sinh(2Hk)]}{5 + 2H^2k^2 + 4\nu_r(2\nu_r - 3) + (3-4\nu_r)\cosh(2Hk)}\right] \tag{22}$$

2.4 The Strain Energy of the Inhomogeneous SMPC

The total strain energy per unit area of the inhomogeneous SMPC U_{total} can be expressed as

$$U_{total} = U_s + U_b + U_r \tag{23}$$

where U_s, U_b, and U_r can be expressed as:

$$\begin{aligned} U_s = \frac{1}{2}\Bigg[&\frac{A_{11}}{16}k^4A^4 + \frac{A_{11}\varepsilon_{11}^0 + A_{12}\varepsilon_{22}^0}{2}k^2A^2 + A_{11}{\varepsilon_{11}^0}^2 \\ &+ 2A_{12}\varepsilon_{11}^0\varepsilon_{22}^0 + A_{22}{\varepsilon_{22}^0}^2\Bigg] \end{aligned} \tag{24}$$

$$U_b = \frac{1}{4}D_{11}k^4A^2 \tag{25}$$

$$U_r = \frac{A^2kE_r}{16(1-\nu_r^2)}\left[\frac{(3-4\nu_r)[-4\overline{H} + 2\sinh(2\overline{H})]}{5 + 2\overline{H}^2 + 4\nu_r(2\nu_r - 3) + (3-4\nu_r)\cosh(2\overline{H})}\right] \tag{26}$$

where $\overline{H} = kH$, which is the dimensionless thickness of the resin. To simplify and facilitate the analysis of the effect of the fiber ply angle on the buckling behaviors of inhomogeneous SMPC laminates, the fiber stacking configuration is assumed to be $[\pm\alpha]_2$. The values of A_{11}, A_{12}, A_{22}, and D_{11} for SMPC laminates with different fiber ply angles at different temperatures are shown in Table S2 (Supplementary Information).

3 Buckling and Post-Buckling Analysis

As seen in Eq. (23), the strain energy U_{total} is a function of the dimensionless thickness $\overline{H}$, the fiber plying angle α, and the temperature T. The strain energy corresponding to the critical buckling state of the inhomogeneous SMPC laminate is minimal. Thus, the critical buckling parameters at different temperatures can be calculated by taking the extreme value of U_{total}.

Before calculating the critical buckling parameters, the influence of $\overline{H}$ on U_r should be studied first. As shown in Fig. 2a, U_r increases monotonically with kH until it gradually approaches a constant value. This demonstrates that the strain energy of the resin matrix increases with increasing matrix thickness. In addition, U_r also increases with increasing ν_r; that is, the incompressibility of the resin matrix contributes to the strain energy of the matrix during buckling. To eliminate the effect of Poisson's ratio of the matrix, we multiply U_r by $(1-{\nu_r}^2)$. The curve of $U_r(1-{\nu_r}^2)$ with respect to the change in kH is shown in Fig. 2b. When $kH > 4.5$, $U_r(1-{\nu_r}^2)$ gradually converges to a constant value $A^2kE_r/8$, which is independent of the thickness of the resin matrix. From the above analysis, it can be seen that when $\overline{H} = 0$, $U_r = 0$, and this problem can degenerate into the buckling process of the composite laminate; when $\overline{H} > 4.5$, the calculated result of U_r is consistent with that of Song's research [31].

In this section, for the convenience of subsequent parameter analysis and optimization design, only the case where $\overline{H} > 4.5$ is considered to obtain the analytical expressions for key parameters, such as the critical buckling strain, buckling wavelength, and buckling amplitude. As shown in Fig. 2, when $\overline{H} > 4.5$, U_r will converge to $\frac{E_r k A^2}{8(1-{\nu_r}^2)}$. Therefore, the total energy U_{total} can be expressed as:

$$U_{total} = c_1k^4A^4 + c_2k^4A^2 + c_3k^2A^2 + c_4kA^2 + c_5 \quad (27)$$

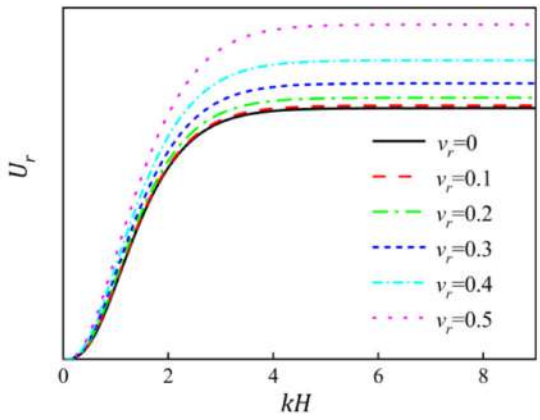

(a)

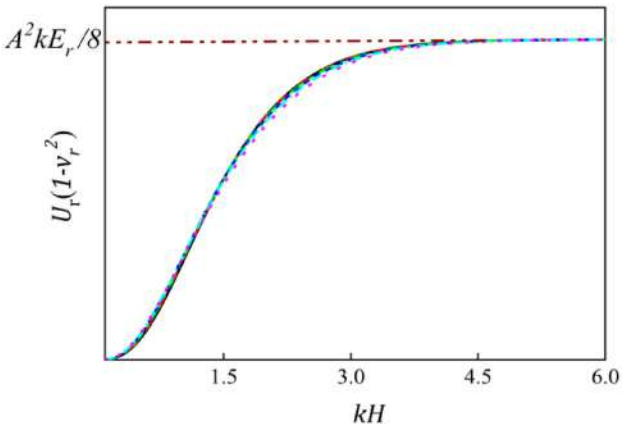

(b)

Fig. 2 **a** The strain energy of the resin matrix U_r and **b** $U_r\left(1-\nu_r^2\right)$ as a function of kH

The coefficients c_i are as follows:

$$\begin{cases} c_1 = \frac{A_{11}}{32} \\ c_2 = \frac{D_{11}}{4} \\ c_3 = \frac{A_{11}\varepsilon_{11}^0 + A_{12}\varepsilon_{22}^0}{4} \\ c_4 = \frac{E_r}{8(1-{\nu_r}^2)} \\ c_5 = \frac{A_{11}{\varepsilon_{11}^0}^2 + 2A_{12}\varepsilon_{11}^0\varepsilon_{22}^0 + A_{22}{\varepsilon_{22}^0}^2}{2} \end{cases} \quad (28)$$

The minimization of the total energy U_{total} with respect to the amplitude A and k requires that

$$\begin{cases} \frac{\partial U_{total}}{\partial A} = 4c_1k^4A^3 + 2\left(c_2k^4 + c_3k^2 + c_4k\right)A = 0 \\ \frac{\partial U_{total}}{\partial k} = 4\left(c_1A^4 + c_2A^2\right)k^3 + 2c_3kA^2 + c_4A^2 = 0 \end{cases} \quad (29)$$

It can be solved that

$$k_c = \left(\frac{c_4}{2c_2}\right)^{\frac{1}{3}} \tag{30}$$

$$A(\varepsilon) = \sqrt{-\frac{c_3}{2c_1 {k_c}^2} - \frac{3c_2}{2c_1}} \tag{31}$$

The critical buckling wavelength can then be calculated as

$$\lambda_c = \frac{2\pi}{k_c} \tag{32}$$

From Eqs. (30)–(32), we can see that there is no prestrain term in the expressions for k_c and λ_c, while the expression for A contains the biaxial prestrain terms. This means that the buckling wavelength does not change with increasing prestrain, while the buckling amplitude varies with the prestrain. In other words, for an inhomogeneous SMPC laminate with a definite fiber stacking configuration, its buckling wavelength under biaxial prestrains is only related to the material properties, while its amplitude will increase monotonically with the prestrains. In addition, the stripe buckling mode can occur in the inhomogeneous SMPC under the influence of in-plane biaxial prestrains only when the following relationship is satisfied:

$$-\frac{c_3}{2c_1 {k_c}^2} - \frac{3c_2}{2c_1} > 0 \tag{33}$$

That is, the biaxial prestrains must satisfy the following relationship:

$$A_{11}\varepsilon_{11}^0 + A_{12}\varepsilon_{22}^0 < -3D_{11}\left[\frac{E_r}{4(1-{\nu_r}^2)D_{11}}\right]^{\frac{2}{3}} \tag{34}$$

Considering the biaxial compressive prestrains, for convenience of the subsequent analysis, we use a factor γ to evaluate the biaxiality, i.e.,

$$\varepsilon_{11}^0 = -\varepsilon,\ \varepsilon_{22}^0 = -\gamma\varepsilon \tag{35}$$

The critical buckling strain can be calculated when $A(\varepsilon) = 0$, and the result is

$$\varepsilon_c = \frac{3D_{11}}{A_{11}+\gamma A_{12}}\left[\frac{E_r}{4(1-{\nu_r}^2)D_{11}}\right]^{\frac{2}{3}} \tag{36}$$

Substituting Eq. (36) into Eq. (31) yields the expression for amplitude A in terms of critical strain and prestrain, i.e.,

$$A = \sqrt{\frac{12D_{11}}{A_{11}+\gamma A_{12}}\left(\frac{\varepsilon}{\varepsilon_c} - 1\right)} \tag{37}$$

It should be noted that the buckling analysis mentioned above is linear buckling analysis, and only basic information about the critical buckling prestrain and wavelength can be obtained. The mechanical equilibrium path (load–displacement curve) of the composite material will bifurcate when buckling. After the bifurcation point, the material will not completely lose its load-bearing capacity but enter the secondary equilibrium path [32]. Therefore, the mechanical behaviors of the material in the process of buckling will be highly nonlinear. When $\varepsilon < \varepsilon_c$, the laminated plate deforms linearly, and the laminate will remain flat ($A = k = 0$), so the buckling amplitude of the composite will be a piecewise function during the uniaxial compression process

$$A = \begin{cases} 0 & \varepsilon \le \varepsilon_c \\ \sqrt{\frac{12D_{11}}{A_{11}+\gamma A_{12}}\left(\frac{\varepsilon}{\varepsilon_c} - 1\right)} & (\varepsilon > \varepsilon_c) \end{cases} \tag{38}$$

So far, the nonlinear buckling behaviors of inhomogeneous SMPC with a fiber stacking configuration of $[\pm\alpha]_2$ under biaxial prestrains have been investigated. The analytical expressions for the critical buckling prestrains and wavelength have been obtained. The evolution of the buckling amplitude with prestrain in the nonlinear buckling process has also been studied. It should be noted that when the fiber stacking configuration is changed (i.e., the tension-bending coupling coefficients need to be considered), only the coefficients c_1, c_2, c_3 and c_4 in Eq. (28) will change, while the subsequent expressions for critical parameters will not change. The analytical expressions for critical buckling strain and wavelength can still be obtained by substituting the changed c_1, c_2, c_3 and c_4 into Eq. (29). Therefore, the method proposed in this paper can be applied to describe the nonlinear buckling behaviors of arbitrary inhomogeneous SMPC under biaxial prestrains.

4 Results and Discussion

4.1 Numerical Verification

Before the parameter study, the commercial software Abaqus should be used first to verify the accuracy of the theoretical analysis proposed in this paper. The detailed descriptions of the finite element model and post-buckling analysis method can be found in Section S2 (Supplementary Information). The mechanical properties of the resin matrix and laminate in the model at different temperatures are the same as those in [33], which are shown in Table S1 (Supplementary Information).

Figure 3 shows the first-order buckling mode of inhomogeneous SMPC with a fiber stacking configuration of $[\pm 30]_2$ at 60°C. The thickness of a single-layer lamina is 0.15 mm, and the thicknesses of the resin matrix are $H = 20h$ and $H = 50h$. The model exhibits a periodic striped buckling morphology on its surface, indicating that the FEA model

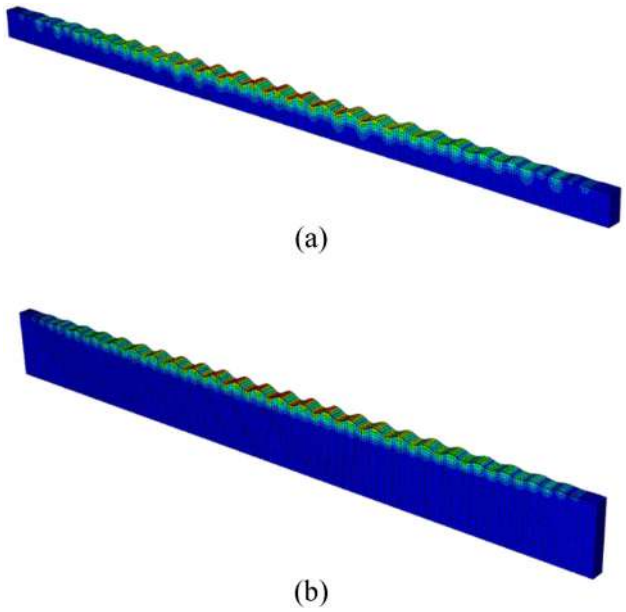

Fig. 3 The first-order buckling mode of inhomogeneous SMPC laminate with a fiber stacking configuration of $[\pm 30]_2$ at 60°C (with a deformation scale factor of 2), **a** $H = 20h$, and **b** $H = 50h$

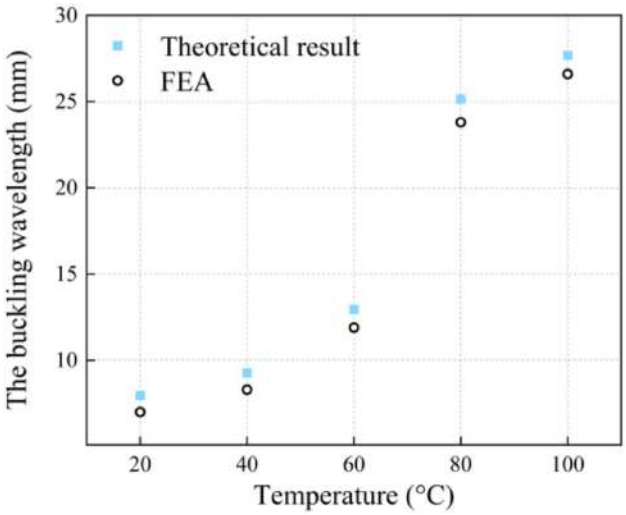

Fig. 4 Comparison between the theoretical and FEA results of the buckling wavelength of inhomogeneous SMPC with a fiber stacking configuration of $[\pm 30]_2$ under different temperatures

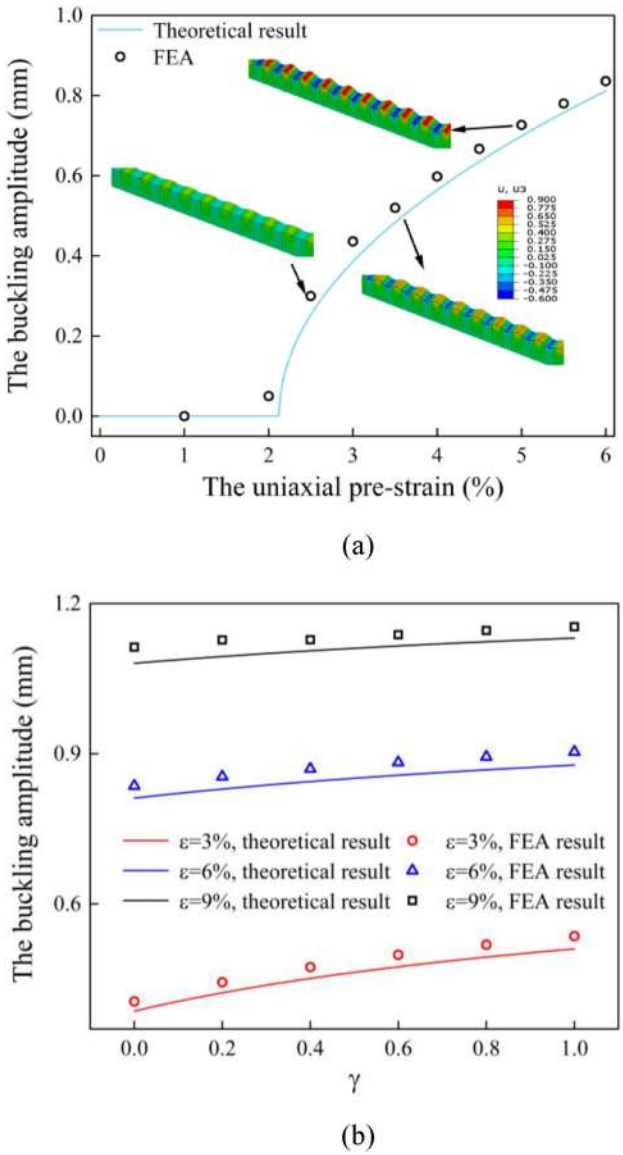

Fig. 5 Comparison between the theoretical and FEA results of the buckling amplitudes of inhomogeneous SMPC with a fiber stacking configuration of $[\pm 30]_2$ at 60°C, **a** $\gamma = 0$, and **b** γ varies from 0 to 1

can effectively simulate the striped buckling mode of the inhomogeneous SMPC. In addition, Fig. 3a, b show that the buckling wavelength is almost independent of the thickness of the resin matrix because kH is already greater than 5 when $H \geq 20h$. Therefore, to improve computational efficiency, the thickness of the matrix will be selected as $H = 20h$ in the subsequent FEA.

Figure 4 shows a comparison between the theoretical and FEA results of the buckling wavelength of the inhomogeneous SMPC laminate with a fiber stacking configuration of $[\pm 30]_2$ at different temperatures. The buckling wavelength predicted by the theoretical solution in this study is in accordance with the simulation result, with an error within 3% at 100°C. This validates the accuracy of the theoretical critical buckling parameters proposed in this article.

The variation of buckling amplitudes with prestrains during the post-buckling analysis is shown in Fig. 5. The fiber stacking configuration remains $[\pm 30]_2$, and the temperature is 60°C. In Fig. 5a, γ is set to 0; that is, we only consider the uniaxial prestrain. The U3 displacement contours of inhomogeneous SMPC under different uniaxial prestrains are also

shown in this figure. It can be seen that the theoretical result shows good agreement with the FEA result when ε is relatively large, while they apparently differ from each other when ε is small. It can also be seen in Fig. 5a that the theoretical $A = 0$ when $\varepsilon < 2.21\%$, while the numerical $A = 0.05$ mm when $\varepsilon = 2\%$. The reason for this phenomenon is that imperfections are introduced in the post-buckling analysis initially, and the laminate will have premature linear buckling deformation, leading to the inaccuracy of the critical buckling strain calculated by FEA, which will be smaller than that of the theoretical result [32]. In other words, with the introduction of initial imperfections, the inhomogeneous shape memory polymer composite laminates will buckle before the prestrain reaches the critical buckling prestrain. Therefore, when the uniaxial prestrain is smaller than the critical buckling prestrain, the buckling amplitude obtained by FEA is greater than 0. However, the variation trend of buckling amplitudes with prestrains obtained through theoretical calculation aligns with the simulation result, and the gap will be reduced to less than 5% with the increase of prestrains.

Besides, Fig. 5b shows the buckling amplitudes of inhomogeneous SMPC laminates as a function of γ with different prestrains obtained from theoretical and FEA. It can be seen that the results obtained through theoretical calculation is in accordance with the simulation result, and the error is within 5%. Therefore, the theoretical method proposed in this study can well predict the buckling and post-buckling behaviors of inhomogeneous SMPC induced by prestrains at different temperatures.

4.2 Parametric Study

The normalized prestrain $\varepsilon/\varepsilon_c$, normalized buckling wavelength λ/h, and normalized buckling amplitude A/h are introduced to facilitate subsequent parametric research.

4.2.1 The Buckling Map

According to Eq. (34), the inhomogeneous SMPC will buckle only when the biaxial prestrains satisfy a certain relation. Thus, the buckling maps of inhomogeneous SMPCs with different fiber stacking configurations at various temperatures are plotted in Fig. 6. The xy coordinates are biaxial prestrains ε_{11}^0 and ε_{22}^0, respectively. The region below the curve represents the inhomogeneous SMPC laminate that will undergo nonlinear buckling deformation at that level of biaxial prestrain; the region above the curve represents the inhomogeneous SMPC laminate that will not buckle at that level of biaxial prestrain. The prestrains corresponding to the curve are the critical buckling prestrains.

As shown in Fig. 6a, for inhomogeneous SMPC laminates with the same fiber stacking configuration, the critical buckling curves at different temperatures are parallel to one another. The area of the post-buckling region increases with increasing temperature, indicating that the inhomogeneous SMPCs can buckle over a wider range of biaxial prestrains as the temperature increases. It can be seen in Fig. 6b that with increasing ply angle α, the area of the nonlinear buckling region decreases in the biaxial prestrain region of $-4.2\% < \varepsilon_{11}^0 < -2\%$ and $-12\% < \varepsilon_{22}^0 < 15\%$, which indicates that inhomogeneous SMPCs are more prone to buckling when $\alpha = 0°$. The buckling maps provide an easy way to determine the buckling state of inhomogeneous SMPC laminates at different biaxial prestrain levels.

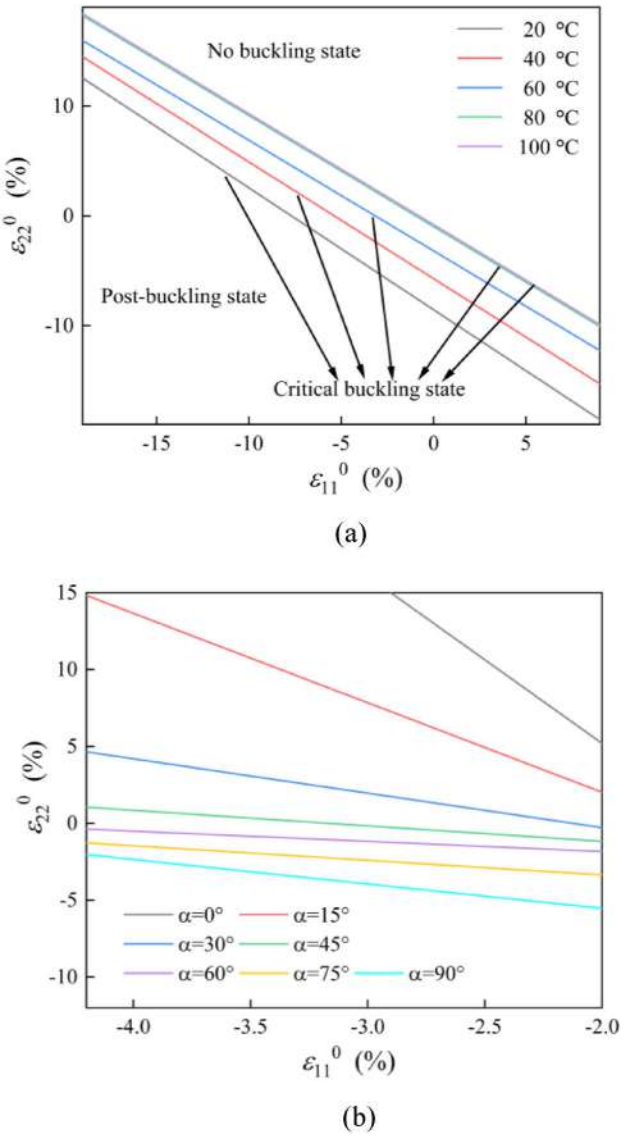

Fig. 6 The buckling maps of inhomogeneous SMPCs: **a** the buckling map of inhomogeneous SMPC with a fiber stacking configuration of $[\pm 45]_2$ at different temperatures, and **b** the buckling map of inhomogeneous SMPC at 60°C with different fiber stacking configurations

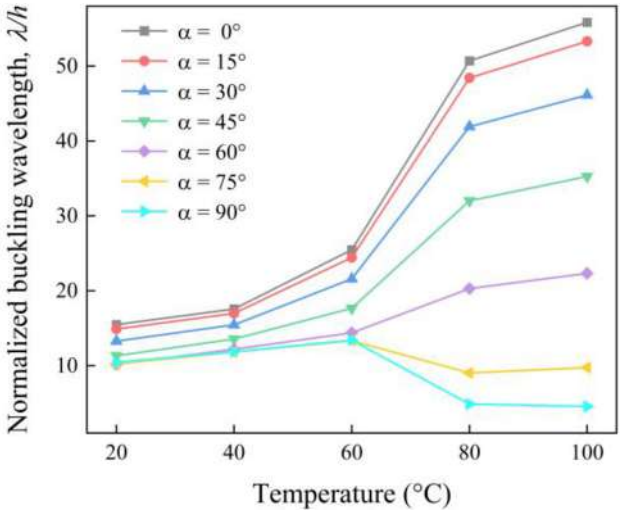

Fig. 7 The normalized buckling wavelength of inhomogeneous SMPC as a function of temperature with different fiber stacking configurations

4.2.2 The Critical Buckling Wavelength

The critical buckling wavelength is independent of prestrains, and only relies on the mechanical properties of the SMPC laminate and SMP matrix. Therefore, it is important to study the influence of ply angle α and temperature on the buckling wavelength before examining other key parameters related to prestrains. It can be seen in Fig. 7 that, in general, the normalized buckling wavelength λ/h increases with increasing temperature and decreases with increasing ply angle α. It should be noted that the influence of α on λ/h is particularly pronounced and unusual when the temperature increases from 60 °C to 80 °C. When α is relatively small, the increasing range of λ/h is significant, but as α increases, the increasing range gradually decreases and even becomes negative. For example, when $\alpha = 0°$ and 15°, the increasing range of λ/h exceeds 100%; as α increases to 60°, the increasing range decreases to 41.2%; and when $\alpha = 75°$ and 90°, λ/h actually decreases.

The reason for this phenomenon is that the critical buckling wavelength of inhomogeneous $[\pm\alpha]_2$ SMPCs is mainly determined by the bending stiffness D_{11} of the SMPC laminate and the modulus E_r of the SMP matrix. When α is relatively small, D_{11} mainly depends on the longitudinal modulus E_{11} of SMPC, which is determined primarily by the modulus of reinforcing fibers. As α increases, the contribution of the transverse modulus E_{22} to D_{11} gradually increases, which is mainly dependent on the modulus of resin. As shown in Table S1 (Supplementary Information), E_{11} only decreases by 23.4% as the temperature increases from 60°C to 80°C, but E_{22} and E_r decrease by 99.5% and 90.9%, respectively. We can also see in Table S2 (Supplementary Information) that when the temperature increases from 60°C to 80°C, D_{11} of the $[\pm0]_2$ laminate decreases from 751 N · mm to 300 N · mm, and the decreasing range is 60%, while the D_{11} of the $[\pm90]_2$ laminate at 60°C and 80°C is 231 N · mm and 0.1627 N · mm, respectively, and the decreasing range is 99.9%. Therefore, with an increase in the ply angle α, the increasing range of λ/h continuously decreases; and when $\alpha = 75°$ and 90°, λ/h actually decreases.

4.2.3 The Critical Buckling Strain

In this section, the influences of prestrain biaxiality γ, ply angle α, and temperature T on critical buckling prestrains ε_c are investigated, and only biaxial compressive prestrains are considered. For convenience, positive values are used to represent compressive strain in the following article. It can be seen in Fig. 8a that with increasing temperature, the critical prestrains decrease continuously, i.e., under the same level of prestrains, the inhomogeneous SMPC is more prone to buckling with increasing temperature. When the temperature increases from 20°C to 80°C, ε_c decreases linearly, with a decreasing range of 87%. However, when the temperature continues to rise to 100°C, ε_c remains almost unchanged. This is because the mechanical properties of SMP are closely related to temperature. With increasing temperature, SMP gradually changes from a glassy state to a rubbery state, and the SMPC laminate and SMP matrix become "soft", so the inhomogeneous SMPC is more prone to undergo out-of-plane buckling under prestrains. When the temperature reaches 80 °C, the SMP has become sufficiently "soft", and the reinforcing fibers become the key factor hindering out-of-plane deformation. However, the mechanical properties of the fiber are almost independent of temperature, so ε_c remains almost unchanged when the temperature continues to increase.

Figure 8b shows the variation in ε_c with α at 60°C. It can be seen that ε_c increases with increasing α, i.e., the inhomogeneous SMPC is more likely to buckle when the ply angle approaches the principal direction of the laminate. In addition, we can also see in Fig. 8 that the critical buckling strain decreases when γ increases from 0 to 1. This indicates that the introduction of biaxial prestrains in the inhomogeneous SMPC is more likely to cause out-of-plane buckling than introducing uniaxial prestrain. Notably, ε_c is almost independent of γ when $\alpha = 0°$. When $\alpha = 0°$, the stress in the 2-direction of the composite is almost entirely borne by the resin, while the contribution of the prestrain applied in the 2-direction to the strain energy is very small, so the effect of ε_{22}^0 on ε_c is almost negligible.

4.2.4 The Buckling Amplitude

According to Eq. (38), the dimensionless parameter A/h is a piecewise function that is related to $\varepsilon/\varepsilon_c$, T, γ, and α.

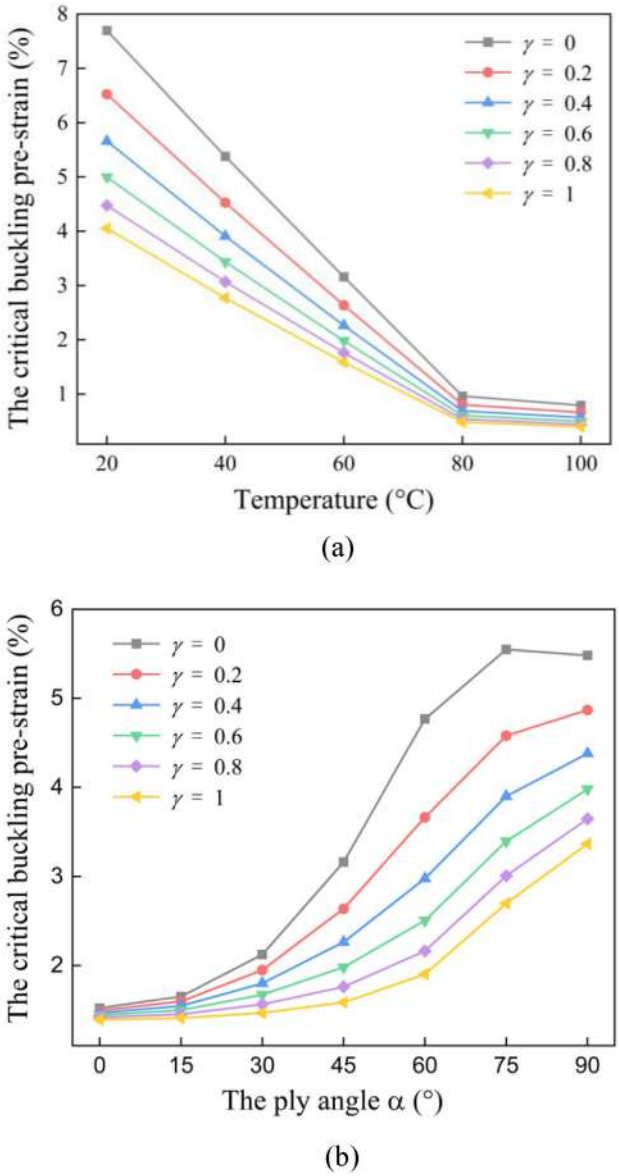

Fig. 8 The critical buckling strain as a function of temperature and ply angle: **a** inhomogeneous SMPC with a ply angle of 45 ° at different temperatures, and **b** inhomogeneous SMPC with different ply angles at 60°C

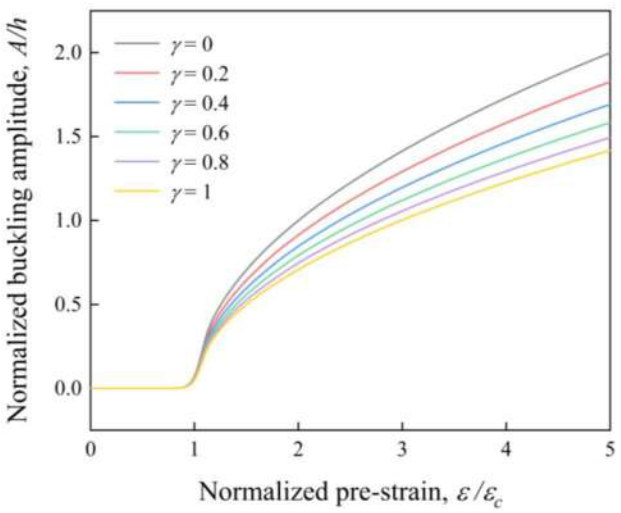

Fig. 9 The normalized buckling amplitude of inhomogeneous SMPC laminate with a ply angle of 45 ° at 60°C as a function of normalized prestrain

The effects of these parameters on the normalized buckling amplitude A/h during the post-buckling process of inhomogeneous SMPC will be studied below. Only biaxial compressive prestrains are considered in this section. The effect of γ on A/h will be investigated first. It can be seen in Fig. 9 that when $\varepsilon/\varepsilon_c < 1$, i.e., the prestrain of the laminate is less than ε_c, only in-plane deformation occurs on the inhomogeneous SMPC, and $A/h = 0$; as $\varepsilon/\varepsilon_c > 1$, A/h increases with increasing prestrain, but the growth rate gradually slows down. In addition, when γ changes from 0 to 1, A/h gradually decreases at the same level of prestrain, indicating that ε_{22}^0 can inhibit the increase in the buckling amplitude during the post-buckling process.

Figure 10a shows the normalized buckling amplitude as a function of temperature when $\alpha = 45°$ and $\varepsilon/\varepsilon_c = 3$. The buckling amplitude of the inhomogeneous SMPC laminate in the post-buckling process is only related to the biaxiality of the prestrains but independent of the temperature. As shown in Fig. 10b, when $\gamma = 0$ (the uniaxial prestrain state), the buckling amplitude is independent of α; when $\gamma \neq 0$, the buckling amplitude decreases first and then increases with increasing α. Therefore, it can be concluded that when $\alpha = 0°$, the buckling amplitude is almost independent of γ; and when $\alpha = 60°$, the buckling amplitude is most sensitive to γ.

5 Design Optimizations by Genetic Algorithm

The influences of ply angle, temperature, and prestrain biaxiality on the critical buckling prestrain, buckling wavelength, and amplitude of the inhomogeneous $[\pm\alpha]_2$ SMPC laminate have been investigated in the previous section. In practice, the buckling deformation of composite materials under the prestrains should be avoided. Therefore, it is necessary to optimize the inhomogeneous SMPC laminate to obtain the corresponding fiber stacking configuration with the maximum critical buckling prestrain.

The optimization design of SMPC laminates is not a simple linear continuous problem, and the optimal fiber stacking configuration cannot be obtained by simply deriving the objective function. In addition, for inhomogeneous

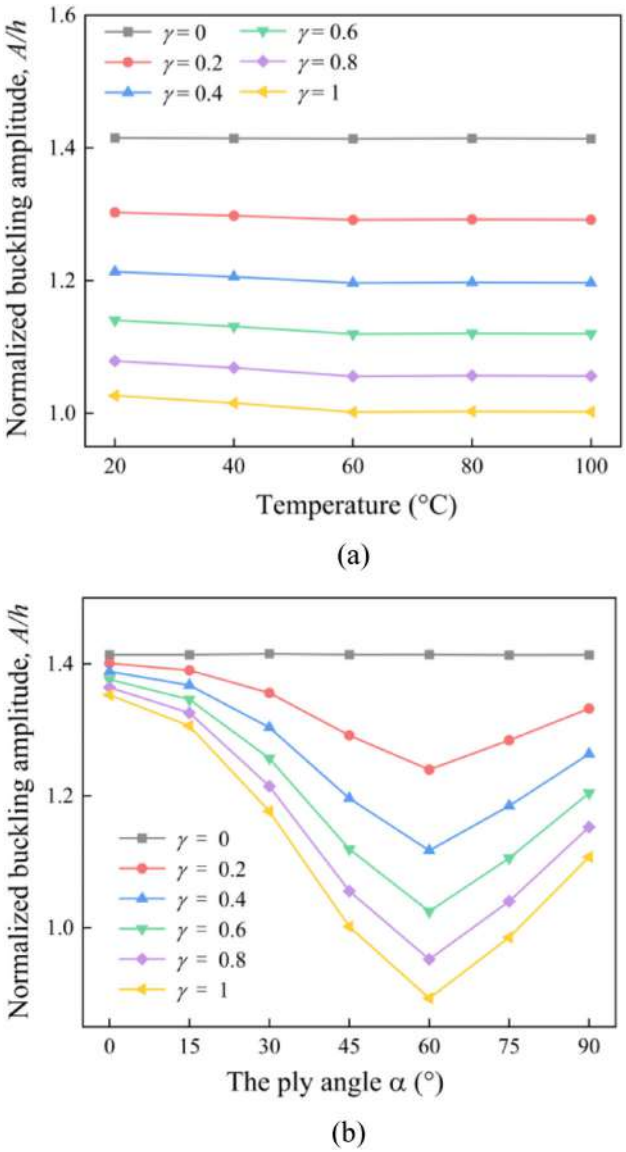

Fig. 10 The normalized buckling amplitude when $\varepsilon/\varepsilon_c = 3$: **a** inhomogeneous SMPC with a ply angle of 45 ° at different temperatures, and **b** inhomogeneous SMPC with different ply angles at 60 °C

SMPC laminates with more layers, i.e., inhomogeneous SMPC laminates with a fiber stacking configuration of $[\pm\theta_1/\pm\theta_2/\pm\theta_3\ldots/\pm\theta_n]$ ($0 < \theta_n \leq 90$, where θ_n is an integer), if the calculation is performed using the exhaustive method in the previous section, the calculation efficiency decreases significantly as the number of layers increases. Therefore, we must find a suitable optimization method to optimize the fiber stacking configurations of inhomogeneous $[\pm\theta_1/\pm\theta_2/\pm\theta_3\ldots/\pm\theta_n]$ SMPCs and find the maximum critical buckling prestrains with different γ to obtain the corresponding optimal fiber stacking configurations.

According to a study by Wei et al. [34], the genetic algorithm (GA) is very suitable for solving optimization problems with discrete design variables, offering excellent global convergence and robustness. In this section, the GA is used to calculate the maximum critical buckling strains of $[\pm\theta_1/\pm\theta_2/\pm\theta_3\ldots/\pm\theta_n]$ under different γ and obtain the corresponding optimal fiber stacking configurations, where $n = 2, 3, 4$, and 5, and $T = 20°C$. The flowchart of the GA is shown in Fig. S2 (Supplementary Information), and the specific parameters for the genetic algorithm are described in Section S3 (Supplementary Information). After several generations of evolution, the maximum critical prestrain of the inhomogeneous SMPC laminate and the corresponding optimal fiber stacking configuration can be obtained.

Figure 11 shows the evolutionary processes of the critical buckling prestrains of inhomogeneous SMPC laminates with different numbers of layers ($\gamma = 0$, $T = 20°C$). The optimal critical prestrains and the average critical prestrains can converge rapidly as the number of layers increases from 4 to 10. When the number of iterations is greater than 15, the average prestrain curve is very close to the maximum prestrain curve, implying that most populations are already in the optimal solution at that time, so the global optimal solution can be obtained rapidly through GA.

Table 1 shows the optimal stacking sequences and corresponding critical buckling prestrains of inhomogeneous SMPC laminates at 20°C. In addition, the influence of γ is also considered. The optimal fiber plying angle is 66° when $\gamma = 0$, which does not change with the increase in the number of layers, i.e., the inhomogeneous SMPC laminate with the fiber stacking configuration of $[\pm 66]_n$ has the strongest resistance to buckling deformation under the uniaxial prestrain state. When $0 < \gamma < 0.4$, the optimal fiber stacking configuration changes with an increase in the number of layers, and the optimal fiber plying angle also increases with an increase in γ. When $\gamma > 0.4$, the optimal fiber plying angle remains at 90 ° regardless of the number of layers. In addition, the maximum critical buckling prestrain of the inhomogeneous SMPC laminate decreases with increasing γ but is independent of the number of layers.

6 Conclusion

In this study, a macroscopic buckling model for inhomogeneous SMPC laminates under initial biaxial prestrains is established. The influences of biaxiality of the prestrains, temperature, and fiber ply angle on the buckling wavelength, critical buckling prestrain, and buckling amplitude are calculated through the energy method. In addition, the optimal fiber stacking configurations of the inhomogeneous SMPC laminates are optimized using a genetic algorithm. The main conclusions of this study are as follows:

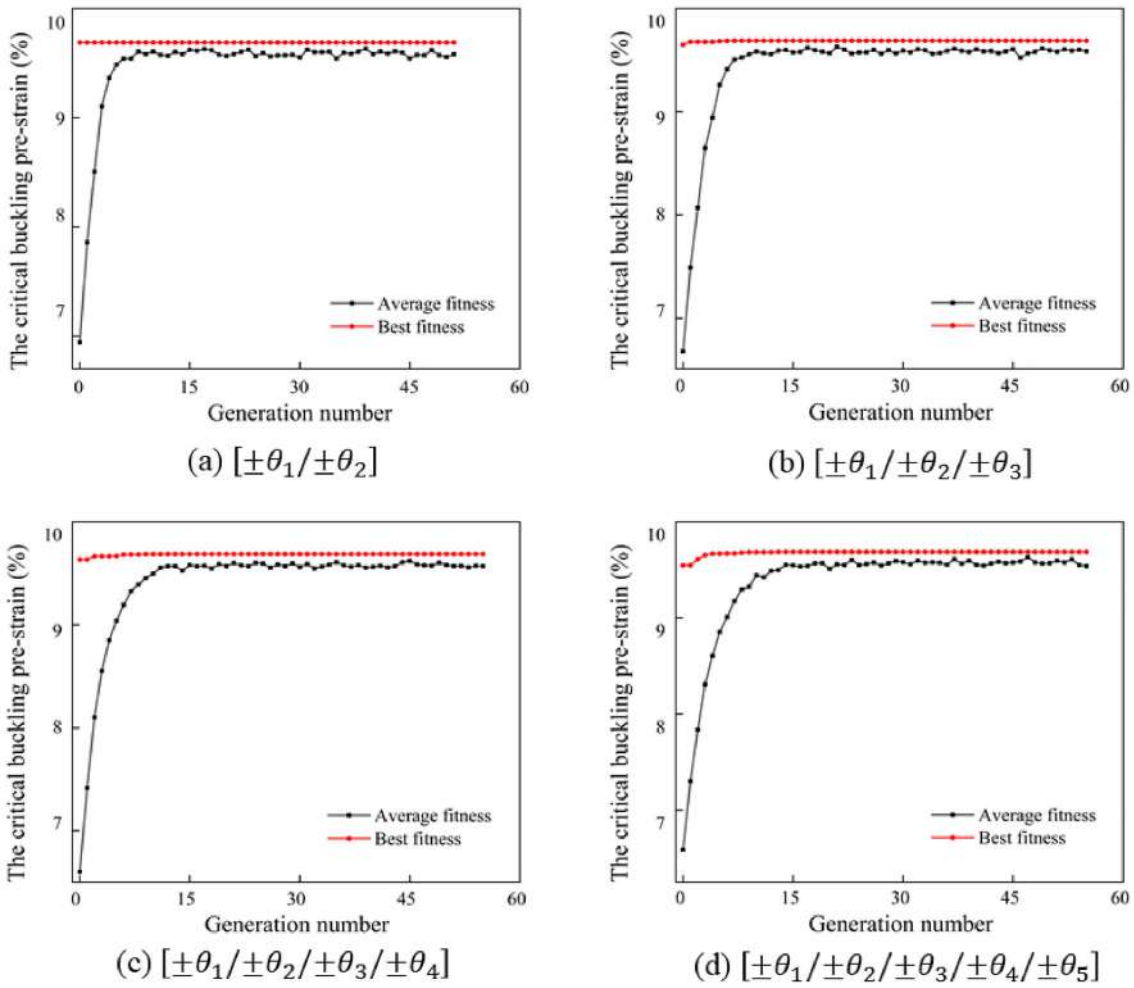

Fig. 11 The evolution of critical buckling prestrain of inhomogeneous SMPC at 20°C using GA

1. When the thickness of the resin-rich region exceeds a certain value ($kH > 4.5$), the strain energy of the resin matrix is only related to the mechanical properties of the resin and the buckling amplitude of the SMPC laminate, which is independent of H.
2. The critical buckling wavelength of the inhomogeneous SMPC laminate is independent of the prestrains, but it increases with increasing temperature and decrease with increasing fiber plying angle. However, when the temperature increases from 60°C to 80°C, the influence of α on λ becomes significantly severe and abnormal.
3. The critical buckling prestrain of the inhomogeneous SMPC laminate decreases with increasing temperature, increasing biaxiality of the prestrains, or decreasing fiber plying angle, while the amplitude decreases with increasing biaxiality of the prestrains, but it is almost independent of temperature.
4. A genetic algorithm is used to calculate the maximum critical buckling prestrains of inhomogeneous SMPC laminates with a fiber stacking configuration of $[\pm\theta_1/\pm\theta_2/\pm\theta_3\ldots/\pm\theta_n]$ under different biaxialities of prestrains and obtain the corresponding optimal fiber stacking configurations. The optimal fiber plying angle is always 66° when $\gamma = 0$; when $\gamma > 0.4$, the optimal fiber plying angle is always 90°; and when $0 < \gamma < 0.4$, the optimal fiber stacking configuration changes with the number of layers and γ. The maximum critical buckling prestrain of the inhomogeneous SMPC laminate decreases with increasing γ but is independent of the number of layers.

Table 1 Optimal stacking sequence and the corresponding critical buckling prestrain of inhomogeneous SMPC at 20°C using GA

Biaxiality of prestrain	Optimal stacking sequence	The critical buckling prestrain (%)
$\gamma = 0$	$[\pm 66/\pm 66]$	9.69
	$[\pm 66/\pm 66/\pm 66]$	9.69
	$[\pm 66/\pm 66/\pm 66/\pm 66]$	9.69
	$[\pm 66/\pm 66/\pm 66/\pm 66/\pm 66]$	9.69
$\gamma = 0.1$	$[\pm 71/\pm 71]$	8.98
	$[\pm 73/\pm 69/\pm 73]$	8.99
	$[\pm 76/\pm 69/\pm 69/\pm 76]$	9.00
	$[\pm 81/\pm 69/\pm 69/\pm 69/\pm 81]$	9.01
$\gamma = 0.2$	$[\pm 82/\pm 82]$	8.55
	$[\pm 90/\pm 73/\pm 90]$	8.59
	$[\pm 90/\pm 74/\pm 74/\pm 90]$	8.60
	$[\pm 90/\pm 75/\pm 73/\pm 75/\pm 90]$	8.60
$\gamma = 0.3$	$[\pm 90/\pm 90]$	8.31
	$[\pm 90/\pm 82/\pm 90]$	8.31
	$[\pm 90/\pm 85/\pm 85/\pm 90]$	8.31
	$[\pm 90/\pm 90/\pm 81/\pm 90/\pm 90]$	8.31
$\gamma = 0.4$	$[\pm 90/\pm 90]$	8.09
	$[\pm 90/\pm 90/\pm 90]$	8.09
	$[\pm 90/\pm 90/\pm 90/\pm 90]$	8.09
	$[\pm 90/\pm 90/\pm 90/\pm 90/\pm 90]$	8.09
$\gamma = 1$	$[\pm 90/\pm 90]$	7.00
	$[\pm 90/\pm 90/\pm 90]$	7.00
	$[\pm 90/\pm 90/\pm 90/\pm 90]$	7.00
	$[\pm 90/\pm 90/\pm 90/\pm 90/\pm 90]$	7.00

Supplementary Information The online version contains supplementary material available at https://doi.org/10.1007/s10338-023-00454-4.

Acknowledgements This work is supported by the National Natural Science Foundation of China (Grant Nos. 12102107 and 12272113) and China National Postdoctoral Program for Innovative Talents (No. BX2021090).

References

1. Zare M, Prabhakaran MP, Parvin N, Ramakrishna S. Thermally-induced two-way shape memory polymers: mechanisms, structures, and applications. Chem Eng J. 2019;374:706–20.
2. Wang XT, Zhang FH, Liu LW, Leng JS, Liu YJ, Zhao XF, et al. A humidity-driven flexible carbon nitride film with multiple deformations. Smart Mater Struct. 2019;28(10):7.
3. Memis NK, Kaplan S. Production of thermal and water responsive shape memory polyurethane nanocomposite filaments with cellulose nanowhisker incorporation. Cellulose. 2021;28(11):7075–96.
4. Dumlu H, Marquardt A, Zirdehi EM, Varnik F, Shen YC, Neuking K, et al. A mechanical analysis of chemically stimulated linear shape memory polymer actuation. Materials. 2021;14(3):21.
5. Pantuso E, De Filpo G, Nicoletta FP. Light-responsive polymer membranes. advanced. Opt Mater. 2019;7(16):35.
6. Roudbarian N, Baniasadi M, Nayyeri P, Ansari M, Hedayati R, Baghani M. Enhancing shape memory properties of multi-layered and multi-material polymer composites in 4D printing. Smart Mater Struct. 2021;30(10):12.
7. Gu JP, Zhang XP, Duan H, Wang MQ, Sun HY. A hygro-thermo-mechanical constitutive model for shape memory polymers filled with nano-carbon powder. Int J Smart Nano Mater. 2021;12(3):286–306.
8. Li FF, Scarpa F, Lan X, Liu LW, Liu YJ, Leng JS. Bending shape recovery of unidirectional carbon fiber reinforced epoxy-based shape memory polymer composites. Compos Part A-Appl Sci Manuf. 2019;116:169–79.
9. Zhang D, Liu LW, Lan X, Leng JS, Liu YJ. Synchronous deployed design concept triggered by carbon fibre reinforced shape memory polymer composites. Compos Struct. 2022;290:15.
10. Zhao F, Zheng XY, Zhou SC, Zhou B, Xue SF, Zhang Y. Constitutive model for epoxy shape memory polymer with regulable phase transition temperature. Int J Smart Nano Mater. 2021;12(1):72–87.
11. Deng YD, Lan X, Leng JS. Unidirectional carbon fiber reinforced cyanate-based shape polymer composite with variable stiffness. Adv Eng Mater. 2022;24(12):2200580.
12. Karunakaran K, Singh SS, Kitey R. Investigating the role of filler shape on the dynamic mechanical properties of glass-filled epoxy composites. Polym Compos. 2022;43:6912–25.
13. Leng JS, Lan X, Liu YJ, Du SY. Shape-memory polymers and their composites: stimulus methods and applications. Prog Mater Sci. 2011;56(7):1077–135.
14. Li FF, Liu YJ, Leng JS. Progress of shape memory polymers and their composites in aerospace applications. Smart Mater Struct. 2019;28(10):23.

15. Dayyoub T, Maksimkin AV, Filippova OV, Tcherdyntsev VV, Telyshev DV. Shape memory polymers as smart materials: a review. Polymers. 2022;14(17):26.
16. Sokolowski WM, Tan SC. Advanced self-deployable structures for space applications. J Spacecr Rocket. 2007;44(4):750–4.
17. Luo L, Zhang FH, Leng JS. Shape memory epoxy resin and its composites: from materials to applications. Research. 2022;2022:25.
18. Liu ZX, Hao SD, Lan X, Bian WF, Liu LW, Li QF, et al. Thermal design and analysis of a flexible solar array system based on shape memory polymer composites. Smart Mater Struct. 2022;31(2):14.
19. Wucher B, Lani F, Pardoen T, Bailly C, Martiny P. Tooling geometry optimization for compensation of cure-induced distortions of a curved carbon/epoxy C-spar. Compos Part A-Appl Sci Manuf. 2014;56:27–35.
20. Svanberg JM, Holmberg JA. An experimental investigation on mechanisms for manufacturing induced shape distortions in homogeneous and balanced laminates. Compos Part A-Appl Sci Manuf. 2001;32(6):827–38.
21. Zhang C, Zhang GL, Xu J, Shi XP, Wang X. Review of curing deformation control methods for carbon fiber reinforced resin composites. Polym Compos. 2022;43(6):3350–70.
22. Sironic L, Murray NW, Grzebieta RH. Buckling of wide struts/plates resting on isotropic foundations. Thin-Walled Struct. 1999;35(3):153–66.
23. Liu X, Liu X, Zhou W. An analytical spectral stiffness method for buckling of rectangular plates on Winkler foundation subject to general boundary conditions. Appl Math Model. 2020;86:36–53.
24. Manshadi BD, Vassilopoulos AP, de Castro J, Keller T. Instability of thin-walled GFRP webs in cell-core sandwiches under combined bending and shear loads. Thin-Walled Struct. 2012;53:200–10.
25. Yang J, Shen HS, Zhang L. Nonlinear local response of foam-filled sandwich plates with laminated faces under combined transverse and in-plane loads. Compos Struct. 2001;52(2):137–48.
26. Cao PY, Niu KM. New unified model of composite sandwich panels/beams buckling introducing interlayer shear effects. Compos Struct. 2020;252:9.
27. Topal U, Trung VD, Dede T, Nazarimofrad E. Buckling load optimization of laminated plates resting on Pasternak foundation using TLBO. Struct Eng Mech. 2018;67(6):617–28.
28. Landau LD, Lifšic EM, Lifshitz EM, Kosevich AM, Pitaevskii LP. Theory of elasticity: volume 7: Elsevier; 1986.
29. Huang ZY, Hong W, Suo Z. Nonlinear analyses of wrinkles in a film bonded to a compliant substrate. J Mech Phys Solids. 2005;53(9):2101–18.
30. Huang SQ, Li QY, Feng XQ, Yu SW. Pattern instability of a soft elastic thin film under van der Waals forces. Mech Mater. 2006;38(1–2):88–99.
31. Song J, Jiang H, Choi WM, Khang DY, Huang Y, Rogers JA. An analytical study of two-dimensional buckling of thin films on compliant substrates. J Appl Phys. 2008;103(1):10.
32. Zhao H, Mu T, Lan X, Liu L, Liu Y, Leng J. Microbuckling behavior of unidirectional fiber-reinforced shape memory polymer composite undergoing compressive deformation. Compos Struct. 2022;297:115975.
33. Zhao H, Lan X, Liu Y, Bhattacharyya D, Leng J. Flexural and shape memory properties of unidirectional glass and carbon fibers reinforced hybrid shape memory polymer composites. Smart Mater Struct. 2022;31(11):115024.
34. Wei RF, Pan G, Jiang J, Shen KC, Lyu D. An efficient approach for stacking sequence optimization of symmetrical laminated composite cylindrical shells based on a genetic algorithm. Thin-Walled Struct. 2019;142:160–70.